Naval Research Laboratory

Washington, DC 20375-5320

NRL/MR/5674--19-9878

Analysis of High-Speed Cameras as Coherent Receivers for Interferometric Sensing Applications

Brandon Redding, Matthew Murray, and Allen Davis

Fiber Optics Technology Branch
Optical Sciences Division

May 9, 2019

REPORT DOCUMENTATION PAGE

Form Approved
OMB No. 0704-0188

1. REPORT DATE *(DD-MM-YYYY)*	**2. REPORT TYPE**	**3. DATES COVERED** *(From - To)*
09-05-2019	Memorandum Report	Sept. 2018 - Mar. 2019

4. TITLE AND SUBTITLE

Analysis of High-Speed Cameras as Coherent Receivers for Interferometric Sensing Applications

5a. CONTRACT NUMBER

5b. GRANT NUMBER

5c. PROGRAM ELEMENT NUMBER

6. AUTHOR(S)

Brandon Redding, Matthew Murray, and Allen Davis

5d. PROJECT NUMBER

5e. TASK NUMBER

5f. WORK UNIT NUMBER
6A94

7. PERFORMING ORGANIZATION NAME(S) AND ADDRESS(ES)

Naval Research Laboratory
4555 Overlook Avenue, SW
Washington, DC 20375-5320

8. PERFORMING ORGANIZATION REPORT NUMBER

NRL/MR/5674--19-9878

9. SPONSORING / MONITORING AGENCY NAME(S) AND ADDRESS(ES)

Naval Research Laboratory 6.2 Basic Program

10. SPONSOR / MONITOR'S ACRONYM(S)

11. SPONSOR / MONITOR'S REPORT NUMBER(S)

12. DISTRIBUTION / AVAILABILITY STATEMENT

DISTRIBUTION STATEMENT A: Approved for public release; distribution is unlimited.

13. SUPPLEMENTARY NOTES

14. ABSTRACT

Recent advances in high-speed digital cameras has enabled their use in a host of interferometric sensing applications previously restricted to photodetector based coherent receivers. In this memo, we derive expressions for the shot and digitization noise limits on the phase noise of a camera based coherent receiver. We analyze the receiver performance in both the strong-LO and equal-LO regimes and experimentally validate the analytic predictions. This analysis illustrates the advantages of camera based coherent receivers and identifies the relevant design considerations.

15. SUBJECT TERMS

16. SECURITY CLASSIFICATION OF:			**17. LIMITATION OF ABSTRACT**	**18. NUMBER OF PAGES**	**19a. NAME OF RESPONSIBLE PERSON**
a. REPORT	**b. ABSTRACT**	**c. THIS PAGE**			Brandon Redding
Unclassified Unlimited	Unclassified Unlimited	Unclassified Unlimited	Unclassified Unlimited	14	**19b. TELEPHONE NUMBER** *(include area code)* (202) 767-2174

Standard Form 298 (Rev. 8-98)
Prescribed by ANSI Std. Z39.18

This page intentionally left blank.

Abstract

Recent advances in high-speed digital cameras has enabled their use in a host of interferometric sensing applications previously restricted to photodetector based coherent receivers. In this memo, we derive expressions for the shot and digitization noise limits on the phase noise of a camera based coherent receiver. We analyze the receiver performance in both the strong-LO and equal-LO regimes and experimentally validate the analytic predictions. This analysis illustrates the advantages of camera based coherent receivers and identifies the relevant design considerations.

Introduction

The recent development of digital cameras supporting frame rates in excess of 10 kHz has inspired a host of work exploring the use of cameras as baseband coherent receivers for a variety of interferometric sensing applications [1–3]. Camera based coherent receivers have several attractive features compared with conventional photodetector based coherent receivers:

First, they enable the detection of multiple spatial modes without compromising mixing efficiency. For example, in many sensing applications, interaction with turbulence or scattering from a rough object causes distortion or even speckle formation in the interrogation beam. In a conventional photodetector based coherent receiver, spatial filters such as single mode fibers are required to enable efficient mixing with a reference arm. This spatial filtering step is not required on a camera based receiver, enabling the receiver to use more of the return light [1]. The spatial mode profile recorded using a camera can also carry additional information which could be used to provide a more accurate measurement [2] or to provide spatial information about a sample in imaging applications [4–8].

Second, cameras are typically capable of detecting much higher peak power than photodetector based receivers. The individual pixels on cameras operate as integrators—collecting any photons incident on the pixel during the exposure time and only saturating when the full well depth is reached. As a result, the saturation threshold for pixels is dictated by the pulse energy rather than the peak power. Thus, for a shorter pulse, a pixel can detect higher peak powers.

To illustrate this advantage, we calculated the maximum peak power, P_{peak}, a typical high speed camera can receive without saturating:

$$P_{peak} = \frac{WD \cdot N_{pix}}{T_{cpi}} \left(\frac{h\nu}{\eta}\right) \tag{1}$$

Where WD is the well depth, N_{pix}, is the number of pixels, h, is Planck's constant, ν, is the optical frequency, T_{cpi}, is the pulse duration or the coherent processing interval, and η is the quantum efficiency. Figure 1 shows the peak power as a function of pulse duration for a high speed, silicon camera operating in the visible spectrum (Vision Research Phantom v2512) and an InGaAs camera operating in the short-wave IR (SWIR) spectrum (Xenics Cheetah). The Vision Research camera is capable of recording 10^6 pixel frames at a rate of 25 kHz and a pixel well depth of 19,500 electrons. Frame rates as high as 1 MHz are possible with a reduced region-of-interest (ROI). The Xenics camera supports 3×10^5 pixel frames with a frame rate of 1700 Hz and a well depth of 8×10^5. Frame rates as high as 80 kHz are possible using a reduced ROI. The peak power required to fill the well depth is shown as a function of pulse duration in Fig. 1 for the two cameras. For nanosecond long pulses, both cameras can receive peak power >1 W without saturating. For comparison, typical COTS photodetectors saturate with peak powers on the order of 1-10 mW.

Manuscript approved April 4, 2019.

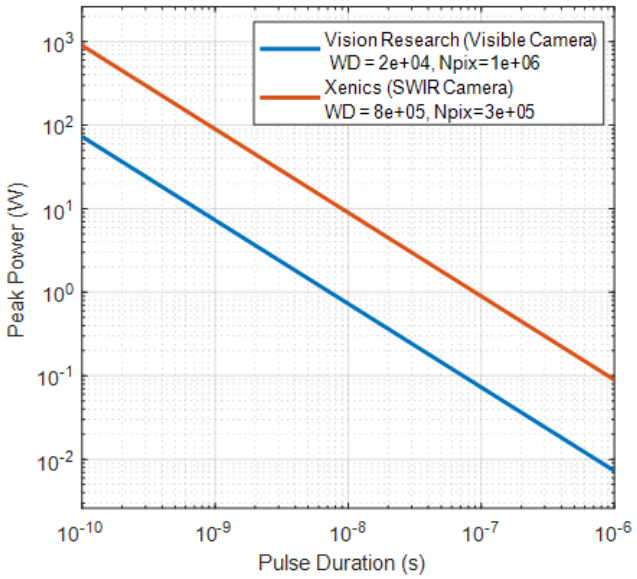

Figure 1. Peak power required to fill the well depth (i.e. saturation threshold) for typical high speed cameras in the visible and SWIR.

Despite recent advances, the primary technical limitation when using a camera based receiver remains the limited frame rate and the minimum exposure time. This is particularly restrictive in distributed sensing applications where a time-gated measurement is required. Even the fastest available cameras exhibit frame rates of only 1 MHz, compared with photodetectors that can easily obtain bandwidths in the multiple GHz range. The minimum exposure time also limits the ability to time gate and is typically restricted to at least 100s of ns. As a result, time-gated experiments may require additional hardware (e.g. acousto-optic modulators (AOMs) or Pockel cells) to achieve high temporal/spatial resolution. Nonetheless, continuing advances in high-speed camera technology are expected to reduce these limitations in the future.

Shot noise limited phase noise derivation:

In this section, we present a derivation of the shot noise limited phase noise for a standard interferometer to highlight the distinction between operations in the strong and equal LO regime.

First, consider the output of a standard interferometer consisting of a sample and reference arm:

$$P_{meas} = P_S + P_R + 2\sqrt{mP_sP_r}\,cos(2\pi f_{IF}t + \Delta\varphi) \tag{2}$$

In this expression, P_{meas} is the power measured on a square law detector, m is the mixing efficiency, P_S is the sample arm power, P_R is the reference arm or LO power, f_{IF} is the intermediate frequency between the sample and reference arm and $\Delta\varphi$ is the relative phase between the two arms. Note that in a baseband receiver the intermediate frequency is typically set to zero. The received optical signal power is converted to an electronic signal power, $\langle i_{IF}^2 \rangle$, which can then be expressed as:

$$\langle i_{IF}^2 \rangle = \left(2\sqrt{mi_si_R}\right)^2 \langle cos^2(2\pi f_{IF}t + \Delta\varphi)\rangle \tag{3}$$

$$\langle i_{IF}^2 \rangle = 2mi_si_R = 2m\left(\frac{\eta q}{h\nu}\right)^2 P_sP_R \tag{4}$$

where m is the mixing efficiency, i_s is the photocurrent generated by the sample arm, i_R is the photocurrent generated by the reference arm, η is the quantum efficiency, and q is the charge of an electron. The noise power due to shot noise can be expressed as:

$$\langle i_{SN}^2 \rangle = 2q(i_s + i_r)B = 2q\left(\frac{\eta q}{h\nu}\right)(P_s + P_R)\frac{1}{T_{cpi}} \tag{5}$$

where B is the processing bandwidth.

Finally, the shot-noise limited CNR can be expressed as:

$$CNR = \frac{\langle i_{IF}^2 \rangle}{\langle i_{SN}^2 \rangle} = \frac{\frac{m\eta}{h\nu}P_S P_R T_{cpi}}{(P_S + P_R)} \tag{6}$$

This CNR expression can then be used to calculate the phase uncertainty per measurement, σ_ϕ, and the phase noise power spectral density (PSD), S_ϕ, for a series of measurements at a sample rate f_s:

$$\sigma_\phi = \frac{1}{\sqrt{2CNR}} \tag{7}$$

$$S_{\phi_{SN}} = \frac{\sigma_\varphi^2}{f_s/2} \tag{8}$$

The phase uncertainty per measurement, σ_ϕ, is units of rad and the phase noise PSD, S_ϕ, is in units of rad^2/Hz.

In many sensing applications, the reference arm is much stronger than the interrogation or signal arm. In this "strong LO regime", we can simplify the CNR expression above by assuming that $P_R \gg P_S$:

$$CNR = \frac{m\eta}{h\nu}P_S T_{cpi} \tag{9}$$

This results in a simplified phase noise PSD expression of:

$$S_{\phi_{SN,strong-LO}} = \frac{1}{mf_s PE_s} \tag{10}$$

where PE_s is the number of photoelectrons resulting from detecting P_s ($PE_s = \frac{\eta}{h\nu}P_S$).

In other applications, the sample arm and reference arm beams have the same power. In this "equal LO regime" ($P_R = P_S$), the CNR expression simplifies as:

$$CNR = \frac{m\eta}{2h\nu}P_S T_{cpi} = \frac{m\eta}{4h\nu}P_{tot} T_{cpi} \tag{11}$$

where $P_{tot} = P_S + P_R$ is the total power received. The phase noise PSD in the equal LO regime is then:

$$S_{\phi_{SN,equal-LO}} = \frac{4}{mf_s PE_{tot}} \tag{12}$$

where PE_{tot} is the number of photoelectrons resulting from detecting P_{tot}. Note the factor of 4 difference between the phase noise PSD in the equal and strong LO regimes. This highlights the advantage of operating in the strong LO regime when a strong LO is available and the number of photoelectrons from the sample arm is much smaller than the camera well depth. However, if there is sufficient light available in both the sample and reference arms to fill the camera well depth, it is advantageous to operate in the equal LO regime.

Digitization noise limited phase noise derivation:

The impact of digitization noise on the CNR of a measurement can be expressed as:

$$CNR = N_{det} M_{sample} 2^{2 \cdot enob} \tag{13}$$

where N_{det} is the number of detectors used (or pixels in the case of a camera), M_{sample} is the number of samples per measurement ($M_{sample} = 1$ per frame for a camera), and $enob$ is the effective number of bits (per pixel). In a camera, the CNR per frame can be written as:

$$CNR = N_{pix} 2^{2 \cdot enob_{used}} \tag{14}$$

where N_{pix} is the number of pixels and $enob_{used}$ is the fraction of the available $enob$ used to measure the interference signal:

$$enob_{used} = enob + \log_2 \left(\frac{2\sqrt{PE_s PE_{LO}}}{PE_{max}} \right) \tag{15}$$

where PE_{max} is maximum number of photoelectrons the camera can record before saturating ($PE_{max} = WD \cdot N_{pix}$). We can then use the digitization noise limited CNR to express the phase noise PSD:

$$S_{\phi_{dig}} = \frac{1}{4 f_s N_{pix} 2^{2ENOB}} \left(\frac{PE_{max}^2}{PE_s PE_{LO}} \right) \tag{16}$$

In the strong LO regime, the reference arm is set to fill the well depth ($PE_{LO} \rightarrow PE_{max}$) and we can write the digitization noise limited phase noise PSD as:

$$S_{\phi_{dig},strong-LO} = \frac{1}{4 f_s N_{pix} 2^{2ENOB}} \left(\frac{WDN_{pix}}{PE_s} \right) \tag{17}$$

$$S_{\phi_{dig},strong-LO} = \frac{1}{4 f_s 2^{2ENOB}} \left(\frac{WD}{PE_s} \right) \tag{18}$$

Remarkably, the dependence on the number of pixels drops out for the strong LO case.

In the equal LO case ($PE_{LO} = PE_s$), we can simplify the phase noise PSD as:

$$S_{\phi_{dig},equal-LO} = \frac{N_{pix}}{f_s \, 2^{2ENOB}} \left(\frac{WD}{PE_{tot}} \right)^2 \tag{19}$$

In this case, the digitization noise not only increases with the number of pixels used, but scales with the square of the number of photoelectrons received in contrast with the linear scaling observed in the strong LO regime.

To illustrate the implications of these expressions, we performed a series of parametric studies on the phase noise PSD in the strong LO and equal LO regimes.

We first consider the strong LO regime. In Fig. 2(a), we show the digitization noise limited PSD as a function of enob. In the strong LO regime, there is no dependency on the number of pixels used; however, the strength of the LO relative to the full well depth does impact the phase noise. As can be seen, using the half the well depth (LO/WD=0.5) results in a 3 dB increase in phase noise at a given enob. The shot noise limit for the same received power ($PE_S = 2 \times 10^6$) is shown in black indicating that shot noise dominates for a camera with enob>7. In Fig. 2(b), we show the ratio of digitization noise to shot noise as a function of enob. In the strong LO regime, this ratio is independent of the sample arm power received or the number

of pixels and is simply a function of the camera enob, well depth, and the fraction of the well depth filled by the LO.

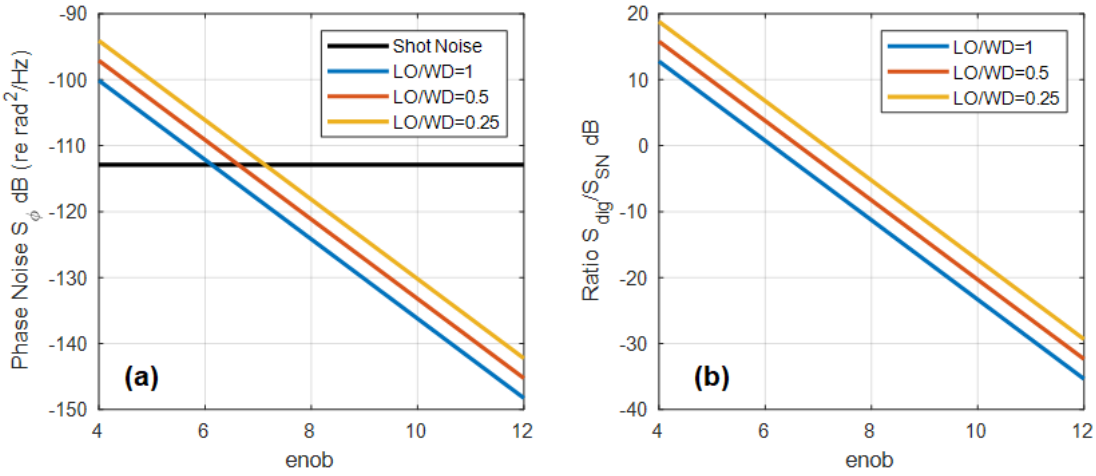

Figure 2. Phase noise analysis in the strong LO Regime. (a) The digitization noise is shown as a function of the enob per pixel for varying LO strength (expressed as a fraction of the full well depth). In this calculation, we assumed a frame rate of 100 kHz, interference patterns recorded across 10^4 pixels, each with a well depth of 19500 and a total of 2×10^6 photoelectrons received. The shot noise limited phase noise is also shown for the same number of photoelectrons received in black. The crossing point indicates that the camera is shot noise limited for an enob>7. (b) The ratio of digitization to shot noise is shown as a function of enob. Note that this ratio is independent of the number of pixels or the number of photoelectrons received in the strong LO regime.

We next consider the equal LO regime. In this case, the digitization noise scales with the square of the received power while the shot noise scales linearly with received power. In addition, the digitization noise depends on the number of pixels used. Fig. 3(a) shows the phase noise due to digitization and shot noise as a function of received power and the number of pixels used. The ratio between the digitization and shot noise is shown in Fig. 3(b). Note that shot noise depends only on the received power level. As a result, it is advantageous to use as few pixels as possible in the equal LO regime without saturating to minimize digitization noise. In addition, digitization noise dominates over shot noise at lower received power levels and thus, higher received power levels will reduce the impact of digitization noise.

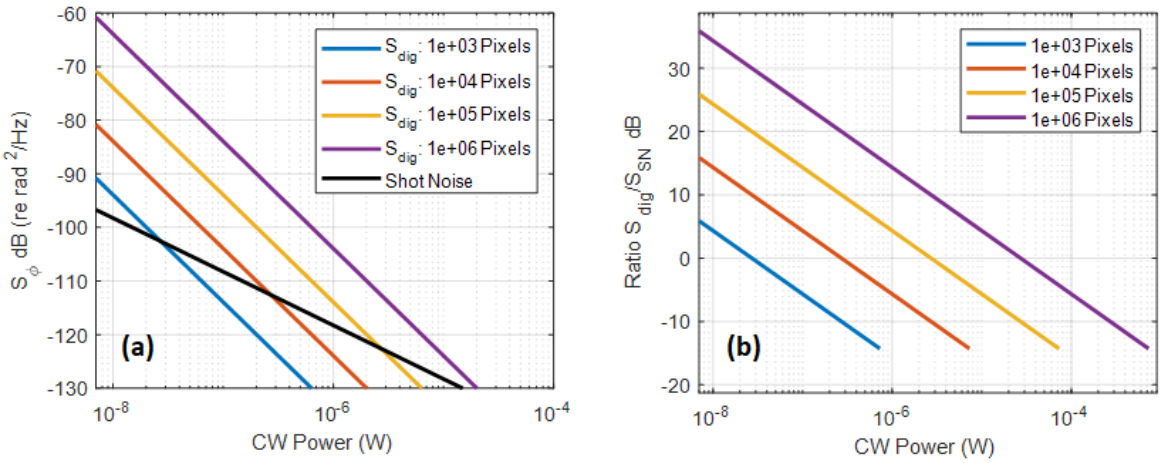

Figure 3. Phase noise analysis in the equal LO Regime. (a) The digitization and shot noise limited phase noise PSD are shown as a function of received power. In this calculation, we assumed a frame rate of 100 kHz, a well depth of 19500, and an enob of 8.5. We also show the digitization noise for varying numbers of pixels. (b) The ratio of digitization to shot noise is shown as a function of the received power and the number of pixels used. Note that the digitization noise plots for a given number of pixels are discontinued when the received power is sufficiently high to saturate the camera. In this case, more pixels are required to detect higher light levels without saturation.

Experimental validation

In order to experimentally validate these predictions we constructed a Mach-Zehnder interferometer as shown in Fig. 4. A narrow linewidth CW laser operating at 532 nm was used as a source and a high-speed camera (Vision Research Phantom v2512) was used to record the relative phase between the two arms of the interferometer using off-axis holography. To test the power dependence in the equal LO regime, a set of neutral density filters was introduced before the interferometer to adjust the total received power. In this case, the power in the two arms remained balanced. In the strong LO regime, neutral density filters were introduced in one arm of the interferometer while the power in the other arm was adjusted using a half wave plate to just fill the camera well depth without saturating. A PZT mounted mirror was used to introduce a known phase modulation for calibration purposes and to confirm that the demodulation continued operate correctly at low light levels.

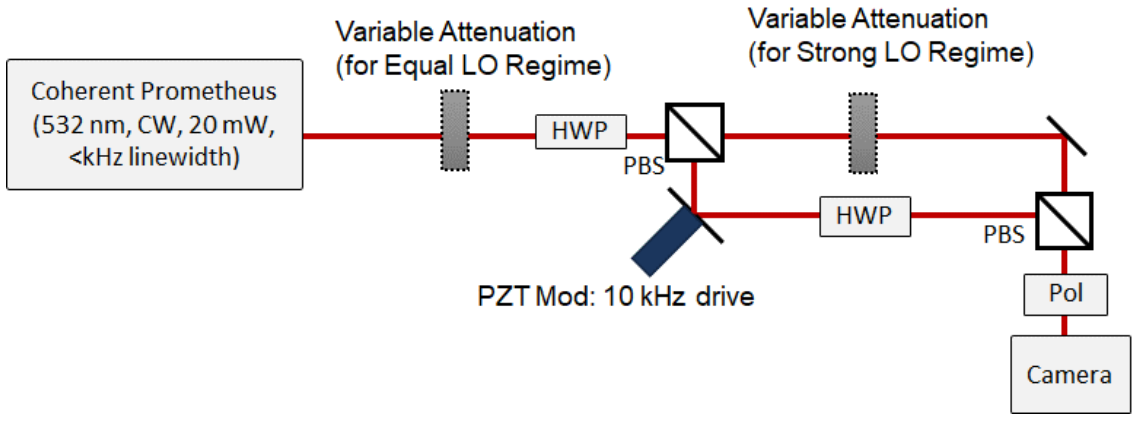

Figure 4. Experimental setup to characterize shot and digitization noise using a camera based coherent receiver.

Before conducting phase noise measurement, we measured the enob of the Vision Research camera by recording 1000 dark images. The enob can be calculated as:

$$enob = log_2\left[\frac{2^{N-bits}}{\sigma_{dark}\sqrt{12}}\right] \tag{20}$$

Where σ_{dark} is the standard deviation of the dark image in units of counts and N-bits is the bit depth of the recorded images (thus 2^{N-bits} is the maximum number of counts and corresponds to the full well depth). The camera was setup to export 16 bit images and has a manufacturer specified bit depth of 12. Our enob calculation is shown in Fig. 5. Fig. 5(a) shows a typical dark image while Fig. 5(b,c) show cross sections through one row and one column over time. The fixed pattern noise in the camera is visible in these cross section images. We then calculated the enob using three methods. First, we calculated σ_{dark} for a single image, providing an enob of 8.53. We then calculated σ_{dark} for the entire datacube of 128×128 pixels images over 1000 frames providing an enob of 8.55. Finally, we calculated the enob separately for each pixel by analyzing the standard deviation of each pixel over 1000 frames. The enob variation across pixels is shown in Fig. 5(d) and the average of the enobs calculated for each pixel was 8.67. Histograms showing the distribution of counts using these three methods are shown in Fig. 5(e,f). In the following, we used an enob of 8.55 to calculate the expected digitization noise for comparison with our experimental measurements.

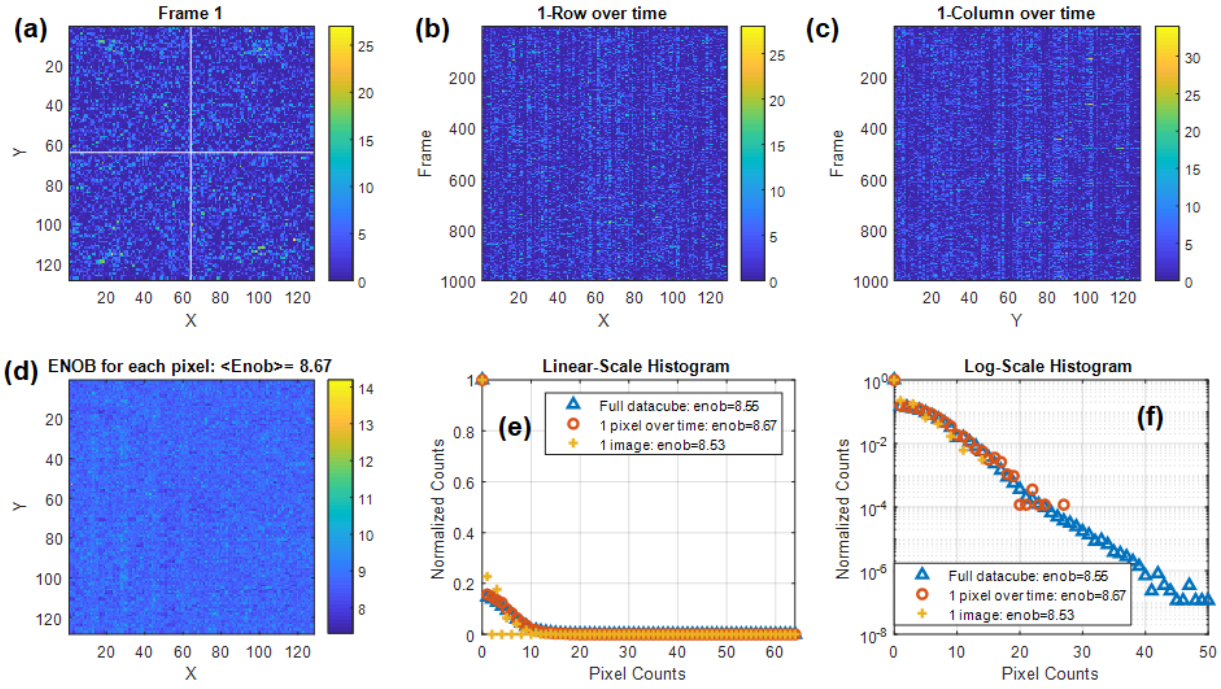

Figure 5. Camera ENOB characterization. (a) A representative dark image. (b) A cross sectional image of one row over 1000 frames. (c) A cross sectional image of one column over 1000 frames. (d) An image where the pixel value represents the enob calculated for a given pixel over 1000 frames. (e) A linear scale histogram of pixel values. (f) A log-scale histogram of pixel values.

Experimental Validation: Strong LO Regime

We then tested the shot and digitization noise dependence on light level in the strong LO regime using the experimental setup shown in Figure 4. We adjusted the relative angle between the sample and reference arm to form an interference pattern on the camera. The camera ROI was set to 10^5 pixels enabling us to computationally select subsets of the recorded ROI (i.e. 10^4 or 10^3 pixel ROIs) to test the dependence on the number of pixels used in post processing. We then adjusted the reference arm power to fill the well depth and recorded 10,000 frames at 100 kHz. An example dataset is shown in Fig. 6. For each frame, we first extracted the relative phase between the two arms using the off-axis holography technique [1]. Figure 6(e) shows the phase noise PSD calculated from the recovered time varying phase using the method described in [1].

In order to estimate the expected shot and digitization noise, we measured the sample arm power level by separately recording an image of the light in just the sample arm (i.e. with the reference arm blocked). A dark image was also recorded and subtracted from the measured sample arm image. By integrating the number of counts in the sample arm only image (less the counts in the dark image), we estimated the number of photoelectrons received (PE_{Rx}) and the power incident on the camera (P_{Rx}) as:

$$PE_{Rx} = N_{counts}\left[\frac{WD}{2^{N-bits}}\right] \tag{21}$$

$$P_{Rx} = \frac{PE}{\eta h\nu} \tag{22}$$

Where N_{counts} is the total number of counts integrated across all pixels in a frame. Note that in the analysis below we set the quantum efficiency in Eq. 22 to unity, and thus the power quoted in the figures below is really the power converted to photoelectrons rather than the power incident on the camera. After calibrating the power on the sample arm, we then used 10 dB neutral density (ND) filters to attenuate the sample arm relative to this calibration measurement. Equations 10 and 18 were then used to estimate the predicted shot noise and digitization noise PSD levels as shown in Fig. 6(e). In the strong LO regime, for an enob of 8.5, the measurement was shot noise limited, with a digitization noise limit 12 dB below the shot noise limit. The experimental measurement was within 2 dB of the combined noise prediction. In Fig. 6(f), we show the experimentally measured phase noise PSD on a plot of the predicted shot and digitization noise vs received power level.

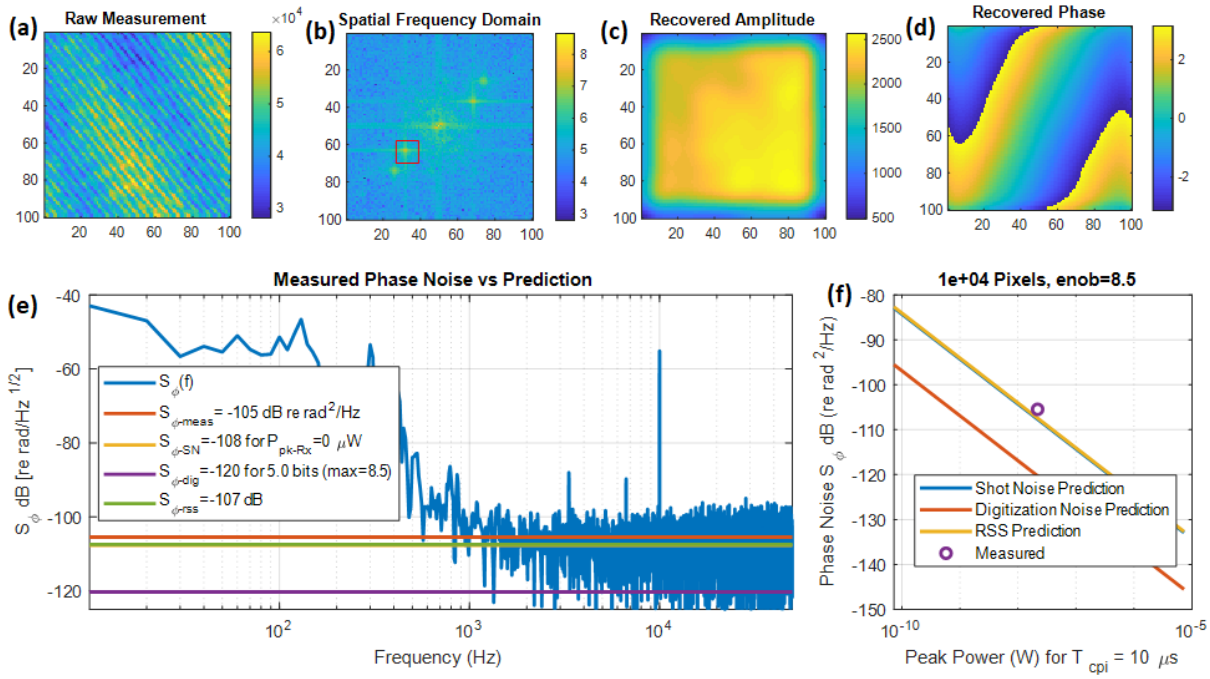

Figure 6. Strong LO regime experimental data. (a) Measured interference pattern. (b) Spatial Fourier transform of the measured interference pattern showing the DC and interference terms. The red box indicates the position of the Hann window applied to select the interference term. (c,d) The recovered amplitude and phase. (e) Measured phase noise PSD compared with the shot, digitization, and RSS (root sum square) noise predictions. (f) The measured phase noise PSD is compared with the predicted noise levels as a function of received power.

We then repeated the above procedure with sample arm power attenuated by 13, 23, and 33 dB with respect to the full well depth. Example interference patterns are shown in Fig. 7(a-c). The phase noise PSDs for these three attenuation levels using a ROI of 10^4 pixels are shown in Fig. 7(d). Note that the tone at 10 kHz due to the PZT is at the same level in each case, confirming that the demodulation operated correctly even at low light levels (nW sample arm power). The noise floor increases with attenuation due to increased shot noise, as expected. We calculated the PSDs for the three attenuation levels by processing the entire 10^5 pixel ROI, or selecting smaller ROIs of 10^4 or 10^3 pixels. In Fig. 7(e), we show the measured phase noise PSD vs received power in a given ROI compared with the RSS (root sum square) predicted phase noise (which is dominated by shot noise in all cases). As expected, in the strong LO regime, there is no dependence on the number of pixels and the phase noise measured with the same number of total photoelectrons (e.g. using 10 dB higher attenuation but 10× more pixels), produced the same phase noise. In addition, the measured data was within 2 dB of the predicted value across 4 orders of magnitude in received power, validating the noise model in the strong LO regime.

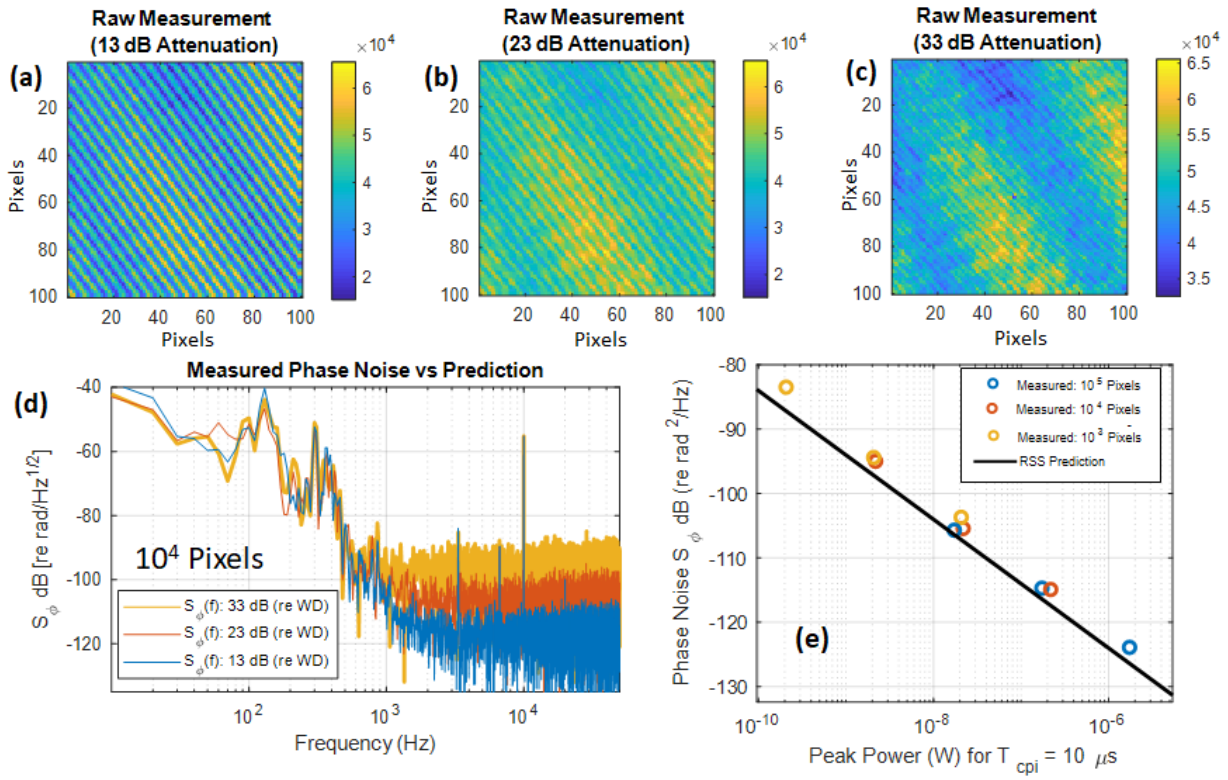

Figure 7. Strong LO regime experimental data. (a,b,c) Interference patterns recorded with 13, 23, 33 dB attenuation with respect to the well depth. (d) Phase noise PSDs with varying attenuation using a 10^4 pixel ROI. Note that the tone at 10 kHz from the PZT modulation is always at the same level. (e) Measured phase noise as a function of received power compared with the RSS predicted phase noise.

Experimental Validation: Equal LO Regime

We then repeated the above experiment in the equal LO regime. In this case, the attenuation was added using ND filters before the interferometer and the power was balanced in both arms. Example interference patterns recorded at varying power levels are shown in Figure 7(a-d). The ROI was set to 10^5 pixels and 10,000 interference patterns were recorded at 100 kHz. The total number of counts in the interference images were used to extract the total number of photoelectrons PE_{tot} and the total received power. A representative phase noise PSD is shown in Figure 7(e). In this case, the digitization noise was 4 dB higher than shot noise. Nonetheless, the measured phase noise was within 1 dB of the predicted RSS value. Figure 8(f) shows the measured phase noise level compared with the shot noise, digitization noise, and RSS prediction.

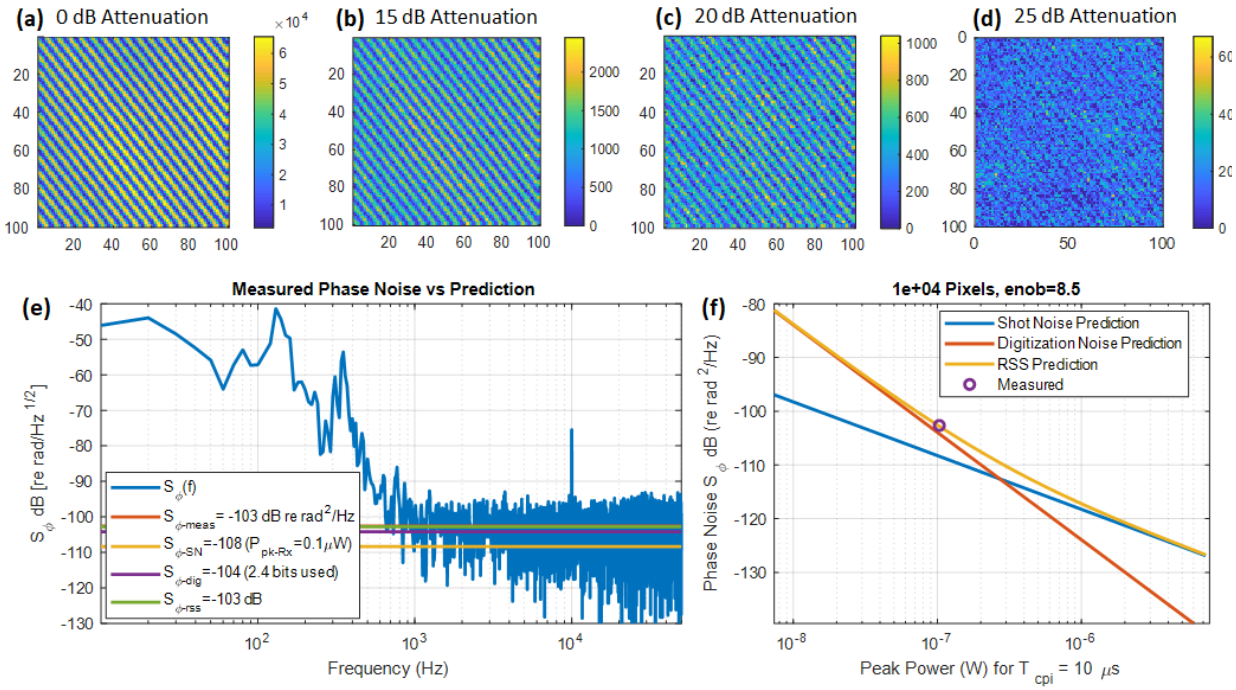

Figure 8. Equal LO Regime experimental data. (a-d) Raw interference patterns recorded at varying attenuation levels (relative to the full well depth). (e) Measured phase noise PSD compared with the shot-noise, digitization, and RSS noise predictions. (f) The measured phase noise PSD is shown in comparison with the predicted noise levels as a function of received power.

We then extracted the phase noise for ROIs of 10^3, 10^4, and 10^5 pixels at varying attenuation levels. Figure 9 shows the extracted phase noise levels vs received power. In the equal LO regime, the shot noise is independent of the number of pixels used, whereas the impact of digitization noise is reduced for smaller ROIs. In addition, the relative contributions of shot and digitization noise depend on the power level with shot noise dominating at higher power levels. The experimental data consistently tracks the predicted curves, confirming our analytic model.

Although we did not include camera dark noise in this analysis, our experimental measurements matched the predicted digitization and shot noise limits. In the strong LO case, the camera dark noise is expected to be negligible, and thus it is not surprising that we achieved shot noise limited with sample arm powers below 1 nW in Fig. 6. However, in the equal LO regime, it is remarkable that measurements with a total power of only 1.5 nW continued to match the digitization noise prediction, indicating that camera dark noise does not have a significant impact on the phase noise at these light levels.

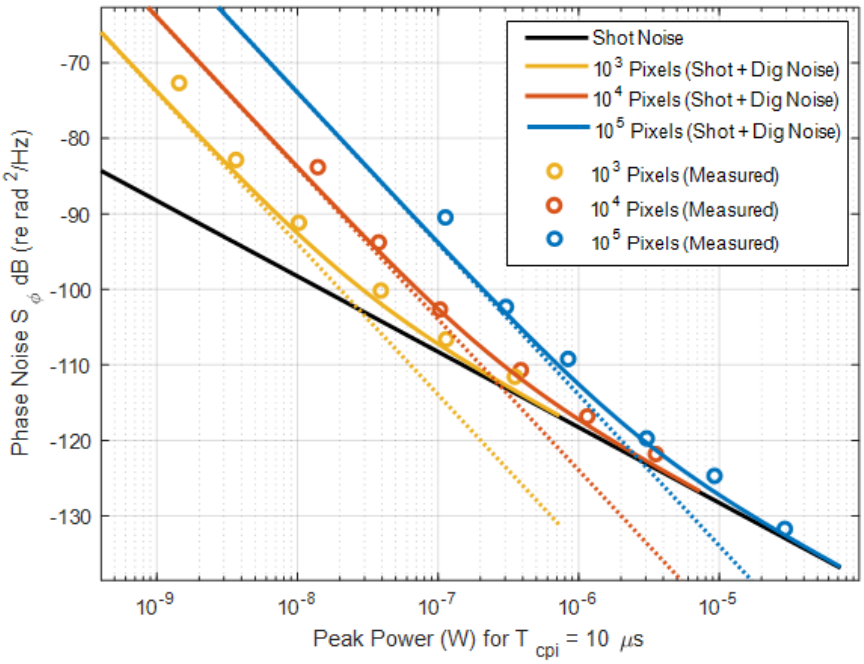

Figure 9. The measured phase noise PSD extracted for varying light level and ROI size compared with the predicted digitization (colored dotted lines), shot (black solid line), and RSS (colored solid lines) noise levels.

Summary

This memo describes the impact of digitization and shot noise on the performance of a camera based coherent receiver in the equal LO and strong LO regimes. We experimentally validated the derived shot and digitization noise expressions and found an excellent agreement with theory. This work can be used to properly design a camera based coherent receiver for interferometric sensing applications.

References

[1] B. Redding, A. Davis, C. Kirkendall, and A. Dandridge, "Measuring vibrational motion in the presence of speckle using off-axis holography," *Appl. Opt.* **55** (2016).

[2] B. Redding and A. Davis, "Measuring vibrational motion from a moving platform using speckle field detection," *Appl. Opt.* **56** (2017).

[3] M. J. Murray, A. Davis, and B. Redding, "Multimode fiber Φ-OTDR with holographic demodulation," *Opt. Express* **26**, 23019 (2018).

[4] A. Dubois and A. C. Boccara, "Full-Field Optical Coherence Tomography" (2008).

[5] J. Poittevin, P. Picart, C. Faure, F. Gautier, and C. Pézerat, "Multi-point vibrometer based on high-speed digital in-line holography," *Appl. Opt.* **54**, 3185 (2015).

[6] F. Bruno, J. Laurent, D. Royer, and M. Atlan, "Holographic imaging of surface acoustic waves," *Appl. Phys. Lett.* **104**, 083504 (2014).

[7] B. Samson, F. Verpillat, M. Gross, and M. Atlan, "Video-rate laser Doppler vibrometry by heterodyne holography," *Opt. Lett.* **36**, 1449–1451 (2011).

[8] G. Pedrini, W. Osten, and M. E. Gusev, "High-speed digital holographic interferometry for vibration measurement.," *Appl. Opt.* **45**, 3456–3462 (2006).